Supplementary Information

Hierarchical Ru Nanoparticles Decorated MoS_2@Ni-MOF for Highly Efficient Overall Water Splitting

Yongyan Xue[a], Jing Chen[a], Jinglin Guo[a], Yueyue Wang[a], Jie Yang[*b], Tuoping Hu[a], and Xiao-Qing Wang[*a]

a. Shanxi Key Laboratory of Hydrogen Energy Carbon Electrode Materials, School of Chemistry and Chemical Engineering, North University of China, Taiyuan 030051, PR China.

b. Shandong Provincial Key Laboratory of Chemical Energy Storage and Novel Cell Technology, and School of Chemistry and Chemical Engineering, Liaocheng University, Liaocheng 252000, PR China.

Materials

The nickel chloride hexahydrate ($NiCl_2 \cdot 6H_2O$) used in the experiment was supplied by Tianjin Beichen Founder. Potassium hydroxide (KOH) was purchased from Da Mao (China) Reagent. The ligand 2-aminoterephthalic acid (2-NH_2-BDC, 98%), sodium molybdate (Na_2MoO_4), and thioacetamide (C_2H_5NS) were all obtained from Aladdin (China) Reagent. Ruthenium(III) chloride ($RuCl_3$) was provided by J&K Scientific Ltd.. Platinum on activated carbon (Pt/C, 20% Pt) was supplied by Beijing Innochem Technology Co., Ltd.. Ruthenium(IV) oxide, anhydrous (RuO_2 powder) was obtained from Alfa Aesar (China) Chemistry Co., Ltd.. Nickel foam (NF, 1.5 mm) was purchased from Taiyuan Lizhiyuan Technology Co., Ltd.. Nafion® 117 solution (~5%) was supplied by Sigma-Aldrich (USA). The nickel foam substrates (1.0 cm × 1.0 cm) were sequentially ultrasonically cleaned in dilute hydrochloric acid, acetone, and deionized water for 15 minutes each to remove surface impurities. All solvents were commercially sourced, and chemical reagents were used as received without further purification.

Synthesis of Ni-MOF-BDC/NF

The Ni-MOF material was synthesized following a previously reported method for NH_2-MIL-101(Ni)[S1]. First, 1.24 mmol of 2-NH_2-BDC was dissolved in 15 mL of DMF to form Solution A. Then, 2.5 mmol of $NiCl_2 \cdot 6H_2O$ was dissolved in 15 mL of DMF to form Solution B. Subsequently, Solution A was added to Solution B, and the mixture was sonicated for 30 minutes to form a homogeneous precursor solution. The mixture was then transferred into a 25 mL Teflon-lined stainless-steel autoclave. A pre-treated piece of nickel foam (NF, 1.0 × 1.0 cm) was immersed in the solution. The autoclave was sealed and maintained at 110 °C for 20 hours. After the reaction, the NF was taken out and thoroughly washed multiple times with DMF and absolute ethanol. Finally, it was dried in a vacuum oven at 60 °C for 8 hours.

Synthesis of MoS_2@Ni-MOF-BDC/NF

0.15 mmol of Na_2MoO_4 and 0.1 mmol of C_2H_5NS were dissolved in 7.5 mL of deionized water. The mixture was ultrasonicated for 10 minutes and then transferred into a 5 mL Teflon-lined stainless-steel autoclave. A piece of Ni-MOF-BDC/NF was vertically immersed in the solution. The autoclave was maintained at 160 °C for 6 hours. After the reaction, the sample was taken out, thoroughly rinsed with deionized water, and dried in a vacuum oven at 60 °C for 8 hours.

Synthesis of Ru_x@MoS_2@Ni-MOF-BDC/NF (X = 0.10, 0.15, 0.20)

For the preparation of $Ru_{0.15}$@MoS_2@Ni-MOF-BDC/NF: 0.15 mmol of $RuCl_3$ was dissolved in 7.5 mL of deionized water. The solution was ultrasonicated at room temperature for 10 minutes, and the precursor MoS_2@Ni-MOF-BDC/NF was vertically immersed in the solution. The reaction was allowed to proceed at 80 °C for 2 hours under static conditions. After the reaction, the electrode was taken out, rinsed with deionized water, and then dried at 60 °C for 8 hours (the average catalyst loading is about 0.5 $mg \cdot cm^{-2}$). When the amounts of $RuCl_3$ added were 0.10 mmol and 0.20 mmol, respectively, the resulting products were denoted as $Ru_{0.10}$@MoS_2@Ni-MOF-BDC/NF and $Ru_{0.20}$@MoS_2@Ni-MOF-BDC/NF.

Synthesis of Pt-C/NF and RuO_2/NF electrodes

3.0 mg of Pt/C or RuO_2 catalyst was dispersed in a mixed solvent consisting of 300 μL deionized water, 300 μL absolute ethanol, and 30 μL of 5% Nafion solution. The mixture was ultrasonicated for 30 minutes to form a homogeneous suspension. Then, 105 μL of the suspension was pipetted and slowly dropped onto the surface of a pre-treated and dried nickel foam (1.0 × 1.0 cm^2). After drying at room temperature, the Pt-C/NF electrode and RuO_2/NF electrode were obtained, with a catalyst loading of approximately 0.5 $mg \cdot cm^{-2}$.

Physical measurements

The crystalline structure of the samples (Ni-MOF-BDC/NF, MoS_2@Ni-MOF-BDC/NF, $Ru_{0.10}$@MoS_2@Ni-MOF-BDC/NF, $Ru_{0.15}$@MoS_2@Ni-MOF-BDC/NF and $Ru_{0.20}$@MoS_2@Ni-MOF-BDC/NF) were analyzed utilizing powder X-ray diffraction (XRD, D/max-2400, Riga ku, Ul-tima IV) with a Cu Kα radiation (λ = 0.154 nm) source, operated at 40 kV and 3 0 mA, within the 2θ range of 5-65°. The morphology and structure of the electrodes were characterized using scanning electron microscopy (SEM). The elements of the electrodes w ere determined by X-ray photoelectron spectroscopy (XPS) measurements (Thermo Scientifi c K-Alpha) and the patterns were collected using Al Kα radiation. For TEM analysis, the electrodes (1 × 1 cm^2) were dispersed ultrasonically in anhydrous ethanol, and the dispersi on was taken for analysis. TEM and HRTEM images were recorded using a JEOL model JEM-2100F (Japan) at an accelerating voltage of 200 kV.

Electrochemical Characterization

All electrochemical measurements were conducted utilizing a CHI660E electrochemical

workstation (Shanghai, Chen Hua) with a conventional three-electrode system in 1.0 M KOH electrolyte and seawater solution at 25°C, in which the graphite rod served as the counter electrode, the as-prepared samples were utilized as the working electrodes, and Ag/AgCl (KCl saturated) was employed as the reference electrode. Before conducting the electrochemical measurement, the catalysts underwent stabilization through 100 cyclic voltammetry (CV) cycles within the potential range of -0.15 to 0.1 mV to ensure consistent performance. The polarization curves were obtained through linear sweep voltammetry (LSV) measurements conducted at a scanning rate of 5 mV s^{-1}, incorporating 90% iR compensation. The Tafel slope was established by graphing the overpotential against the logarithm of current density (log |J|). All potentials reported in the work were converted relative to reversible hydrogen electrode (RHE) according to the Nernst equation ($E_{RHE} = E_{Ag/AgCl} + 0.198+ 0.059 \times pH$). By plotting the difference between the anode and cathode current density ($\Delta j = ja - jc$) at half the potential of CV measurement and the scan rate, the linear slope obtained is twice that of the double layer capacitance (C_{dl}). The ECSA value can be calculated by the formula ECSA = $C_{dl}/Cs*A$, where Cs is the specific capacitance using the average value of 0.04 mF cm^{-2}, A is the actual surface area of the electrode. The solution resistance was obtained from the electrochemical impedance spectroscopy (EIS), which was performed at applied potential with frequency range of 10 mHz-105 kHz condition of 10 mV sinus amplitude for both the HER and OER. The long durability was performed through the chronopotentiometric measurement.

Table S1 HER, OER overpotentials, overall water splitting potentials at 10 mA cm^{-2} and stability times compared with previous reports.

Sample	Electrolyte	HER Over Potential (mV)	OER Over Potential (mV)	Overall Water Splitting Potential (V)	Ref.
$Ru_{0.15}$@MoS_2@Ni-MOF-BDC/NF	1.0 M KOH	53	175	1.53	This work
Fe-MOF@MoS_2-6h	1.0 M KOH	118	187	1.52	2
Ru-CoMOF@MoS_2	1.0 M KOH	289	340	1.59	3
Ru Fe-MOF-PA_{60}	1.0 M KOH	37	217	1.49	4
CoRu-MoS_2	1.0 M KOH	52	308	1.67	5
Ru/Ni/Co@NC	1.0 M KOH	34	174	1.44	6
0.1Fe-NiS/MoS_2	1.0 M KOH	120	297	1.66	7
$CoFe_2O_4$/MoS_2	1.0 M KOH	154	161	1.54	8
CoS_2-MoS_2HNAs/Ti	1.0 M KOH	82	266	1.56	9
HMS/MoS_2/Co_9S_8-31	1.0 M KOH	127	280	1.56	10
Fe-doped Co-LDH@MoS_2-Ni_3S_2/NF	1.0 M KOH	95	220	1.54	11

Table S2 HER fitting results of EIS for Ni-MOF-BDC/NF, MoS_2@Ni-MOF-BDC/NF, Ru_x@MoS_2@Ni-MOF-BDC/NF (x = 0.10, 0.15 and 0.20) and Pt-C/NF.

Sample	R_s (ohm)	R_{ct} (ohm)
Ni-MOF-BDC/NF	1.60	3.08
MoS_2@Ni-MOF-BDC/NF	1.42	1.51
$Ru_{0.10}$@MoS_2@Ni-MOF-BDC/NF	1.55	0.46
$Ru_{0.15}$@MoS_2@Ni-MOF-BDC/NF	1.30	0.44
$Ru_{0.20}$@MoS_2@Ni-MOF-BDC/NF	1.40	0.47
Pt-C/NF	1.70	2.17

Table S3 OER fitting results of EIS for Ni-MOF-BDC/NF, MoS_2@Ni-MOF-BDC/NF, Ru_x@MoS_2@Ni-MOF-BDC/NF (x = 0.10, 0.15 and 0.20) and RuO_2/NF.

Sample	R_s (ohm)	R_{ct} (ohm)
Ni-MOF-BDC/NF	1.37	4.06
MoS_2@Ni-MOF-BDC/NF	1.47	1.32
$Ru_{0.10}$@MoS_2@Ni-MOF-BDC/NF	1.56	1.48
$Ru_{0.15}$@MoS_2@Ni-MOF-BDC/NF	1.45	0.81
$Ru_{0.20}$@MoS_2@Ni-MOF-BDC/NF	1.52	1.11
RuO_2/NF	1.53	6.59

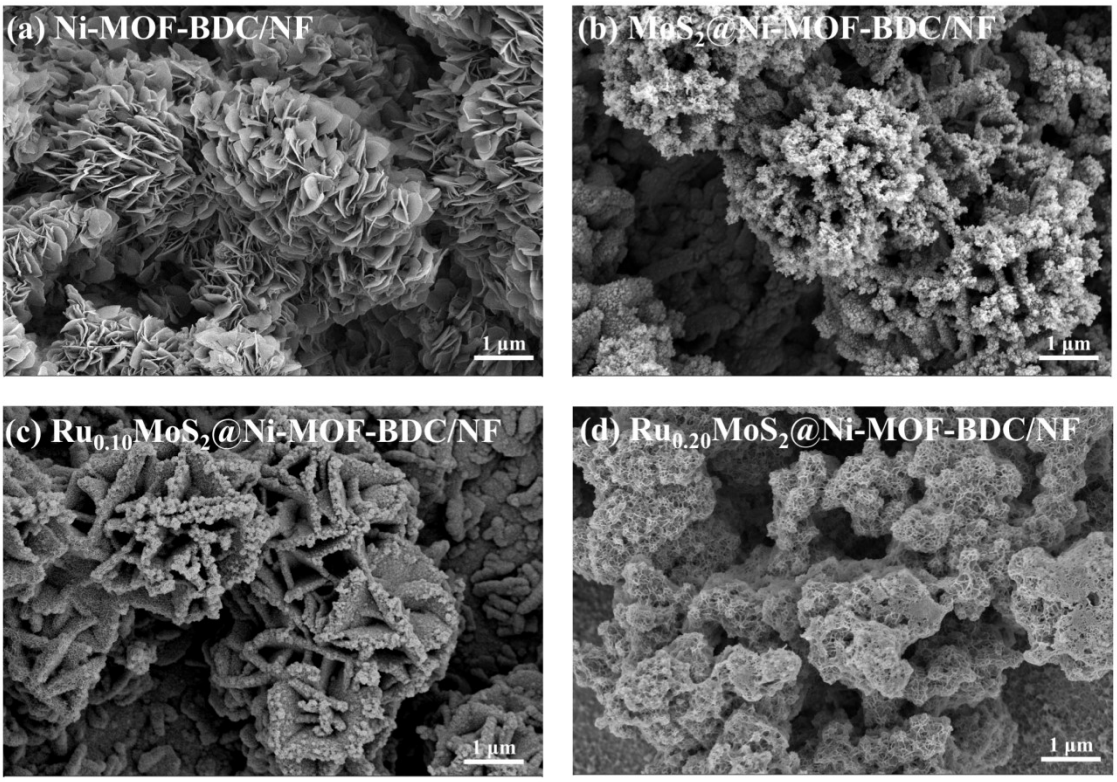

Fig. S1 SEM images of (a) Ni-MOF-BDC/NF; (b) MoS_2@Ni-MOF-BDC/NF; (c) $Ru_{0.10}$@MoS_2@Ni-MOF-BDC/NF; (d) $Ru_{0.20}$@MoS_2@Ni-MOF-BDC/NF

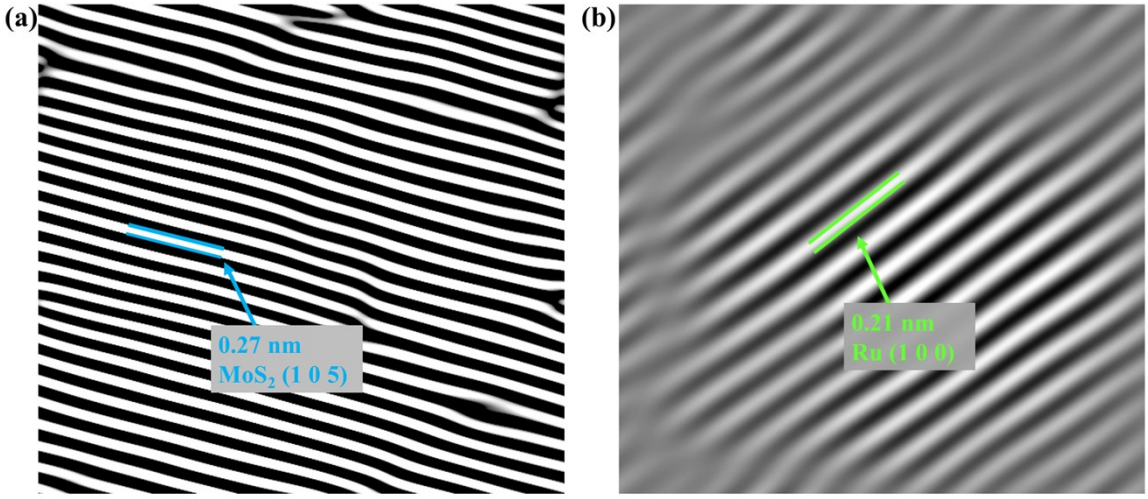

Fig. S2 IFFT images of $Ru_{0.15}$@MoS_2@Ni-MOF-BDC/NF

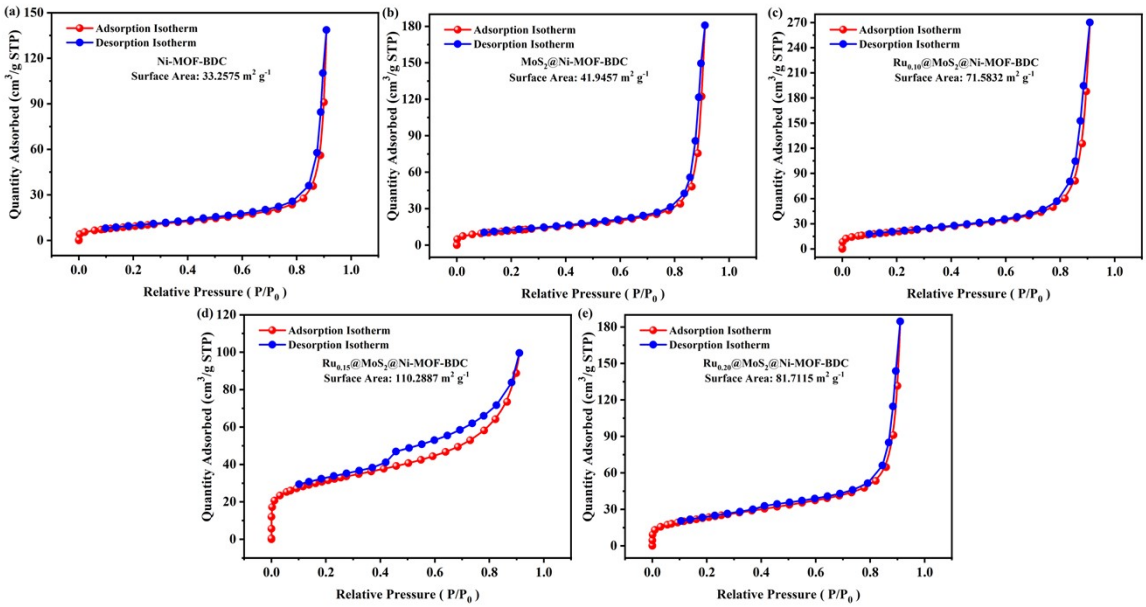

Fig. S3 The N_2 adsorption-desorption isotherm of Ni-MOF-BDC, MoS_2@Ni-MOF-BDC and Ru_x@MoS_2@Ni-MOF-BDC (X= 0.10, 0.15, 0.20) at 77 K.

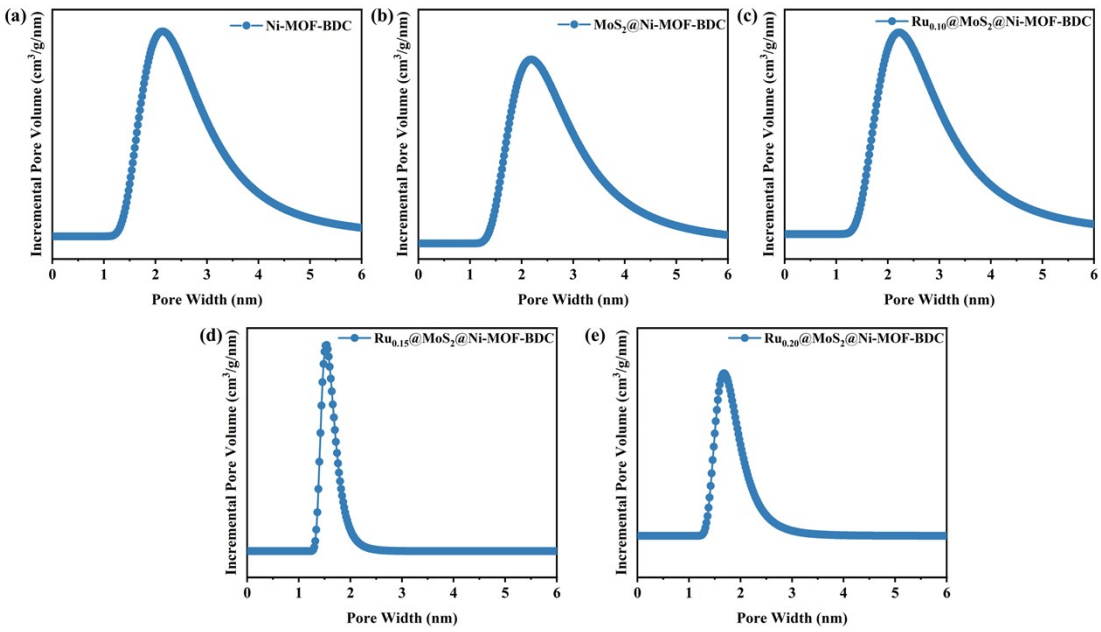

Fig. S4 The pore size distribution curves of Ni-MOF-BDC, MoS_2@Ni-MOF-BDC and Ru_x@MoS_2@Ni-MOF-BDC (X= 0.10, 0.15, 0.20).

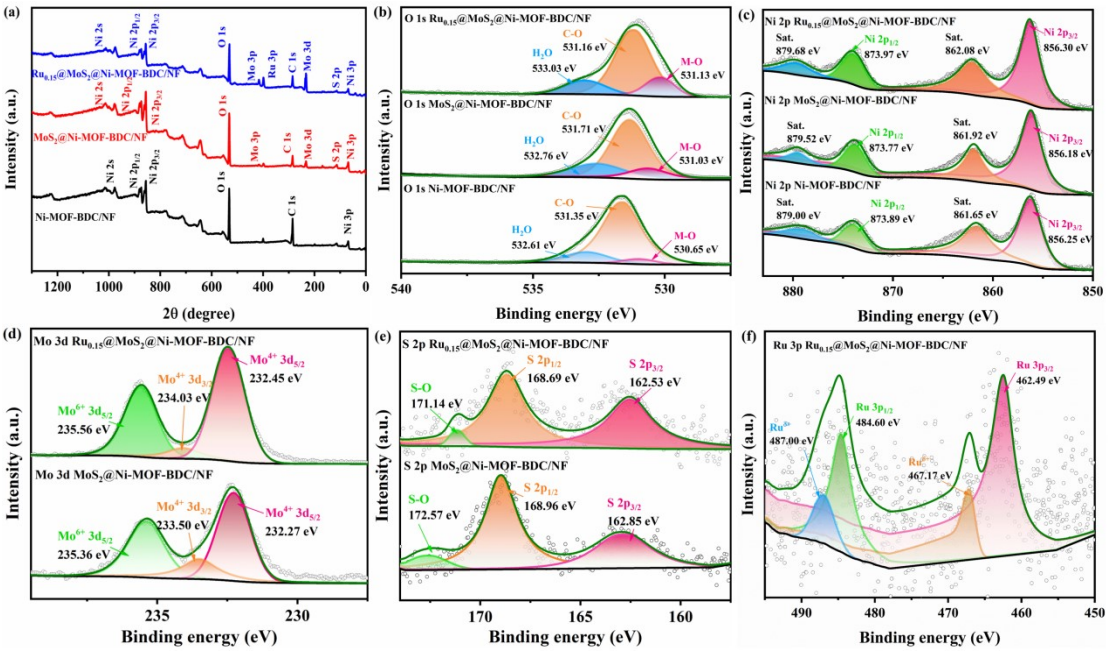

Fig. S5 (a) XPS survey spectra of Ni-MOF-BDC/NF, MoS_2@Ni-MOF-BDC/NF and $Ru_{0.15}$@MoS_2@Ni-MOF-BDC/NF; (b-f) The high-resolution XPS spectra of O 1s, Ni 2p, Mo 3d, S 2p, Ru 3p

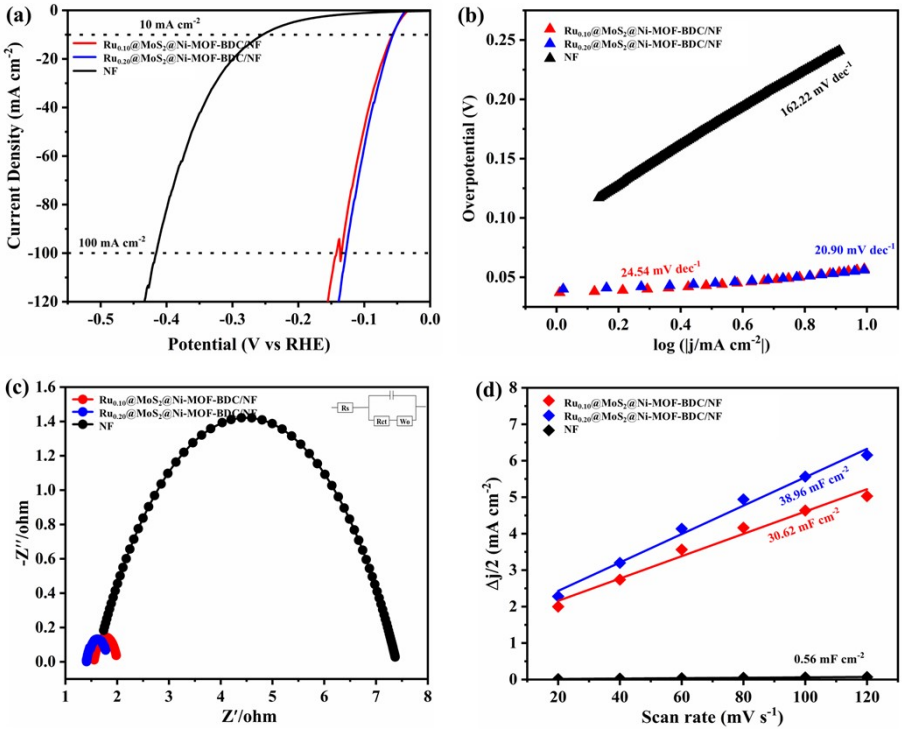

Fig. S6 (a) LSV curves of Ru_x@MoS_2@Ni-MOF-BDC/NF (x = 0.10 and 0.20) and NF; (b) Tafel plots, (c) EIS of $Ru_{0.10}$@MoS_2@Ni-MOF-BDC/NF, $Ru_{0.20}$@MoS_2@Ni-MOF-BDC/NF and NF electrocatalysts (inset: fitted equivalent circuit), (d) C_{dl} value during HER process

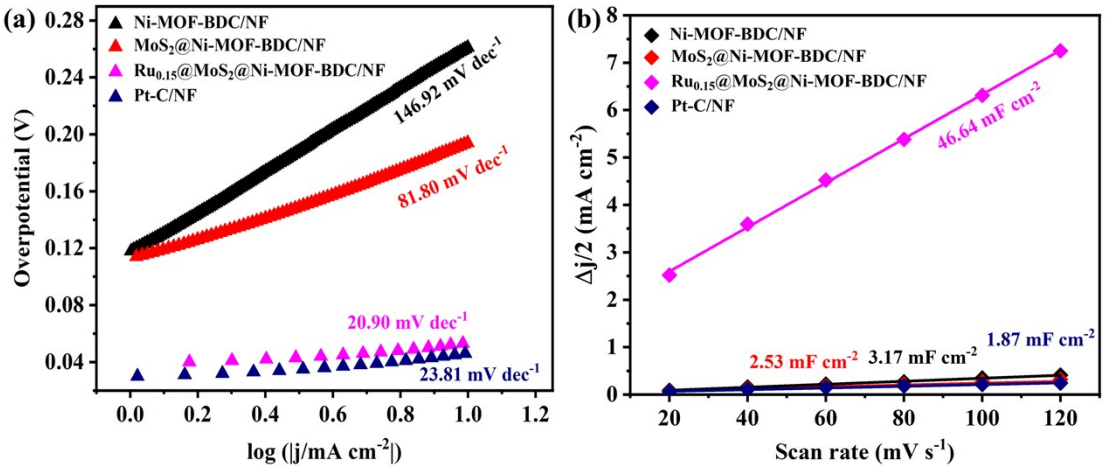

Fig. S7 (a) Tafel plots, (e) Cdl value derived from CV curves for HER process

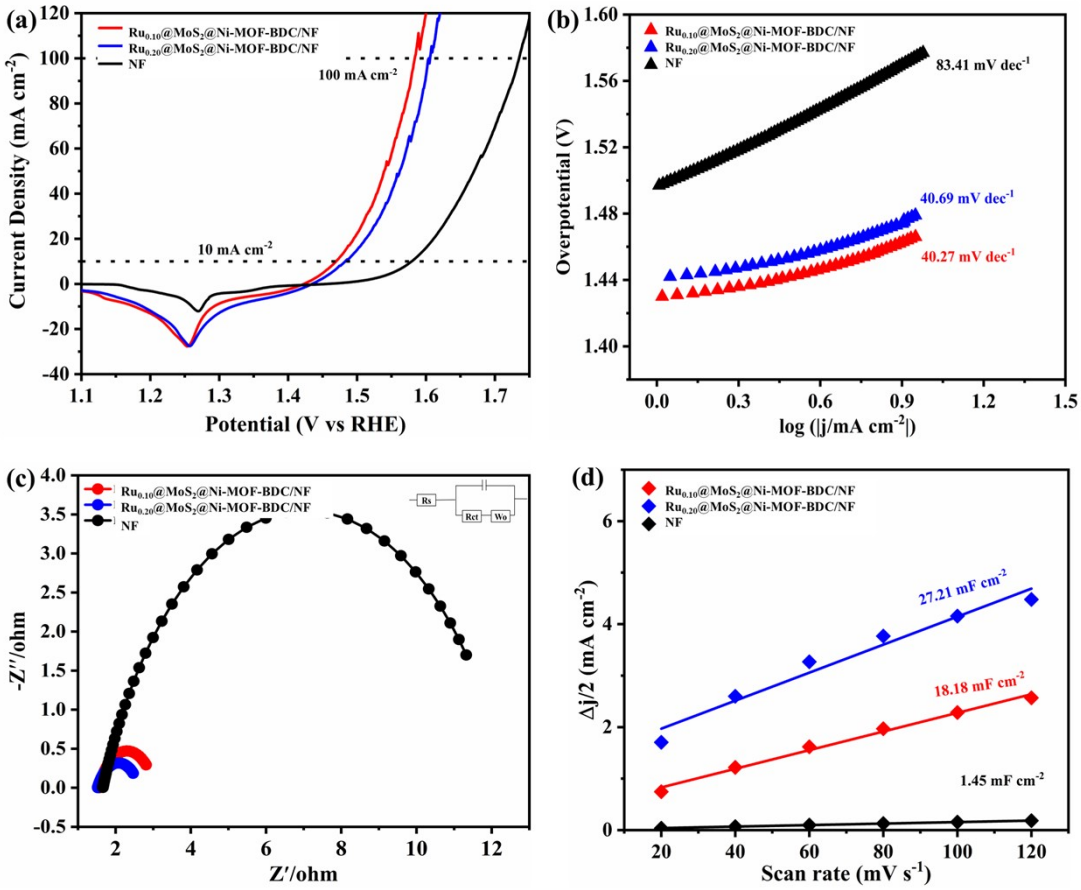

Fig. S8 (a) LSV curves of $Ru_x@MoS_2@Ni$-MOF-BDC/NF (x = 0.10 and 0.20) and NF; (b) Tafel plots, (c) EIS of $Ru_{0.10}@MoS_2@Ni$-MOF-BDC/NF, $Ru_{0.20}@MoS_2@Ni$-MOF-BDC/NF and NF electrocatalysts (inset: fitted equivalent circuit), (d) C_{dl} value during OER process

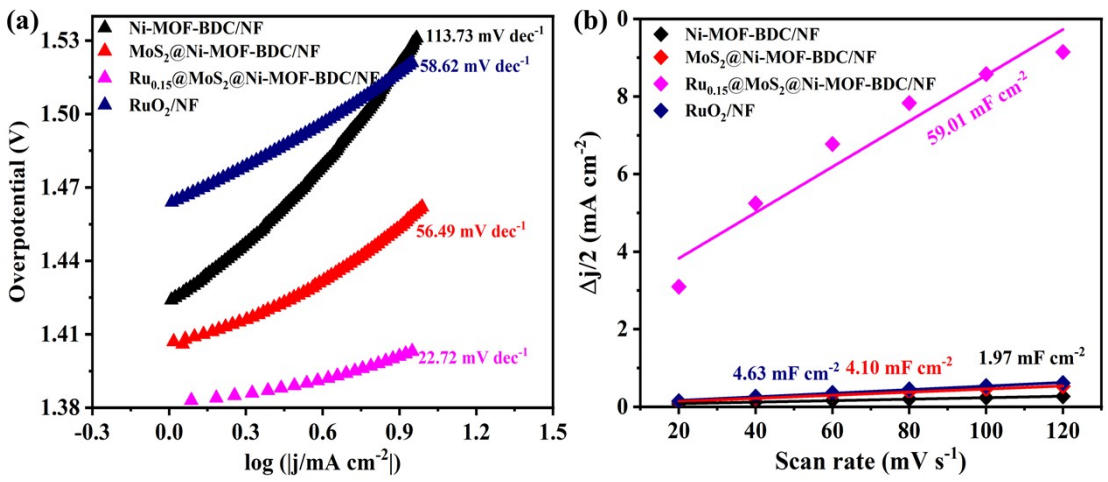

Fig. S9 (a) Tafel plots, (e) Cdl value derived from CV curves for HER process

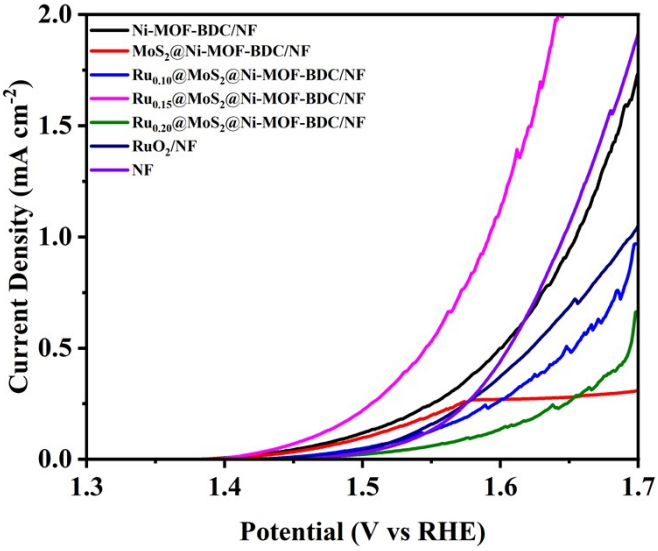

Fig. S10 Polarization curves

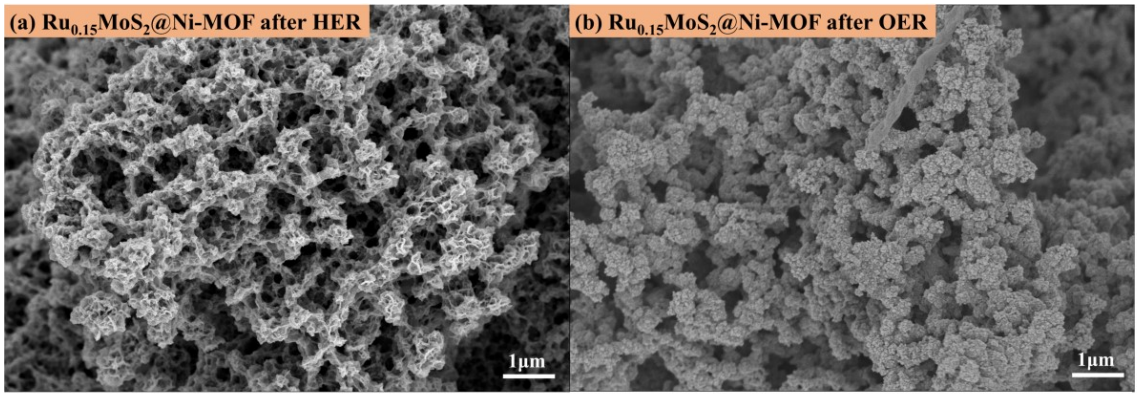

Fig. S11 The SEM images of $Ru_{0.15}$@MoS_2@Ni-MOF-BDC/NF after the HER (a) and OER (b) tests.

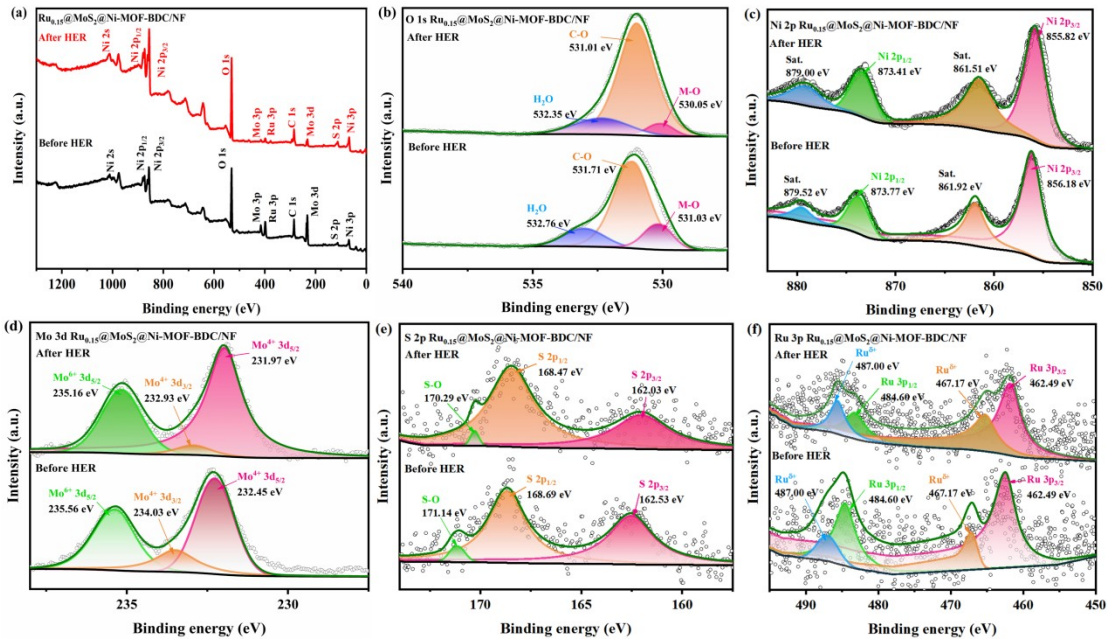

Fig. S12 The XPS spectra of $Ru_{0.15}$@MoS_2@Ni-MOF-BDC/NF before and after the HER test: (a) the survey spectra, (b) O 1s, (c) Ni 2p, (d) Mo 3d, (e) S 2p and (f) Ru 3p.

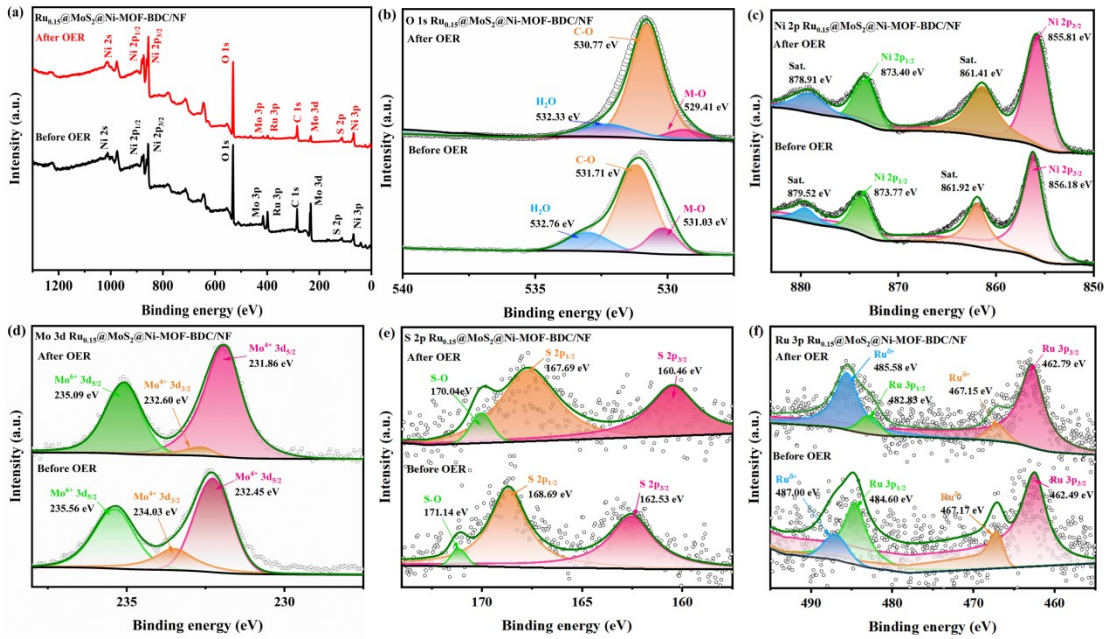

Fig. S13 The XPS spectra of $Ru_{0.15}$@MoS_2@Ni-MOF-BDC/NF before and after the OER test: (a) the survey spectra, (b) O 1s, (c) Ni 2p, (d) Mo 3d, (e) S 2p and (f) Ru 3p.

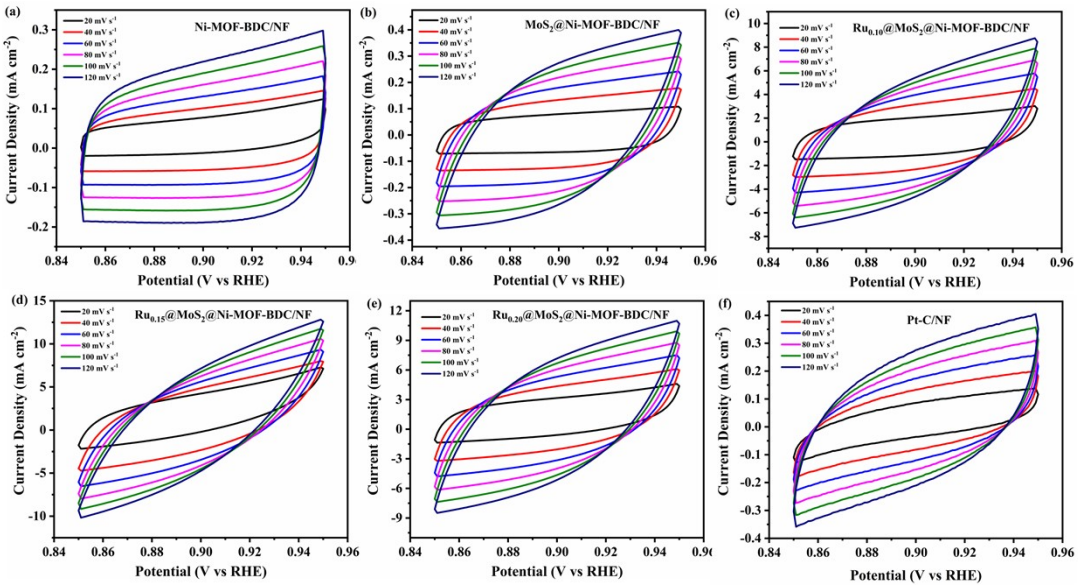

Fig. S14 (a-f) The HER-CV curves for Ni-MOF-BDC/NF, MoS_2@Ni-MOF-BDC/NF, Ru_x@MoS_2@Ni-MOF-BDC/NF (x = 0.10, 0.15 and 0.20) and Pt-C/NF.

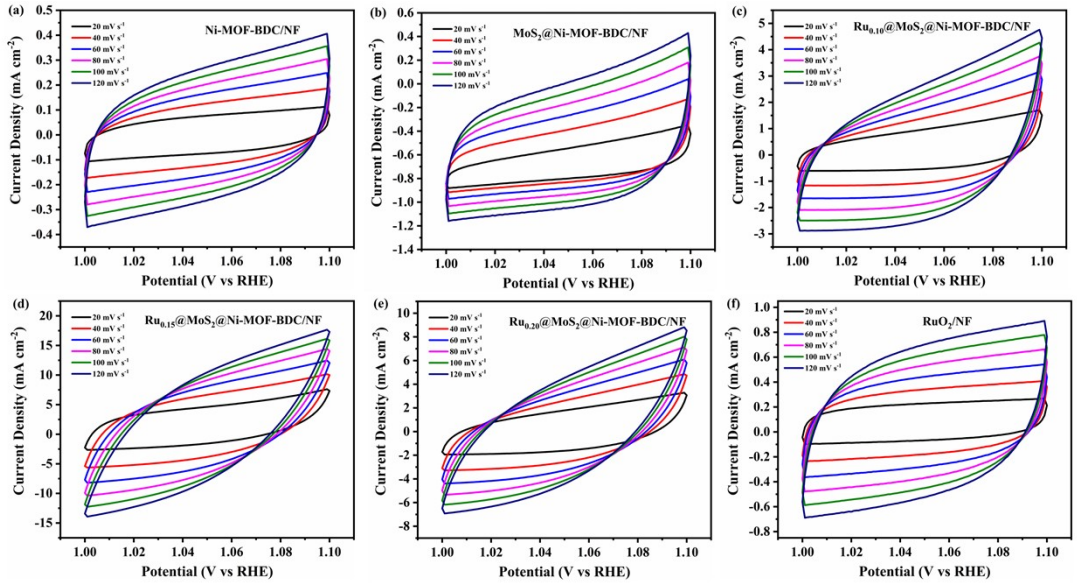

Fig. S15 (a-f) The OER-CV curves for Ni-MOF-BDC/NF, MoS_2@Ni-MOF-BDC/NF, Ru_x@MoS_2@Ni-MOF-BDC/NF (x = 0.10, 0.15 and 0.20) and RuO_2/NF.

References

1. D. Liu, H. Xu and Y. Du, *J Mater Chem A*, 2021, **9**, 24670-24676.
2. R. Velayutham, C.J. Raj and B.C. Kim, *Mater Today Nano*, 2023, **24**, 100387.
3. B.F. Banti, M. Goddati and J. Lee, *ChemSusChem*, 2025, **18**, e202402533.
4. W. Sun, J. Hu and J. Chen, *Mater Today Chem*, 2025, **50**, 103241.
5. I.S. Kwon, T.T. Debela and H.S. Kang, *Small*, 2020, **16**, 2000081.
6. A. Salah, H.-D. Ren and Q.A. Drmosh, *ACS Appl Mater Interfaces*, 2024, **16**, 60310-60320.

7. P. Liu, J. Li and W. Song, *Phys Chem Chem Phys*, 2022, **24**, 8344-8350.
8. Y. Duan, Z. Guo and J. Zhang, *J Colloid Interface Sci*, 2025, **680**, 541-551.
9. Y. Li, W. Wang and H. Wang, *J Energy Chem*, 2021, **57**, 99-108.
10. F. Amiripour,S. Ghasemi, *Fuel*, 2023, **346**, 128299.
11. U. Phadikar, G. Sanyal and T. Kuila, *ChemSusChem*, 2024, **17**, e202400821.